chemosensors

Article

A Flow-Through Biosensor System Based on Pillar[3]Arene[2]Quinone and Ferrocene for Determination of Hydrogen Peroxide and Uric Acid

Dmitry Stoikov [1], Insiya Shafigullina [1], Dmitry Shurpik [1], Ivan Stoikov [1] and Gennady Evtugyn [1,2,*]

[1] A.M. Butlerov' Chemistry Institute, Kazan Federal University, 18 Kremlevskaya Street, Kazan 420008, Russia; dmistojkov@kpfu.ru (D.S.); inzshafigullina@kpfu.ru (I.S.); dnshurpik@mail.ru (D.S.); ivan.stoikov@mail.ru (I.S.)

[2] Analytical Chemistry Department, Chemical Technology Institute, Ural Federal University, 19 Mira Street, Ekaterinburg 620002, Russia

* Correspondence: gennady.evtugyn@kpfu.ru

Abstract: Simple and reliable electrochemical sensors are highly demanded in medicine and pharmacy for the fast determination of metabolites and biomarkers of diseases. In this work, a flow-through biosensor system was developed on the base of a screen-printed carbon electrode modified with pillar[3]arene[2]quinone and ferrocene implemented in carbon black. The modification was performed in a single step and resulted in the formation of a stable layer with good operation characteristics. Uricase was immobilized on the inner walls of a replaceable reactor by carbodiimide binding. A flow-through cell was manufactured by 3D printing from poly(lactic acid). The flow-through system was first optimized on the hydrogen peroxide assay and then used for the determination of 1 nM–0.1 mM uric acid (limit of detection 0.3 nM, 20 measurements per hour). Implementation of ferrocene resulted in a synergetic increase in the cathodic current of H_2O_2 reduction measured by flow switching in chronoamperometric mode. The developed system was tested on the determination of uric acid in artificial urine and Ringer–Locke solution and showed a recovery rate of 96–112%. In addition, the possibility of determination of H_2O_2 in commercial disinfectants was shown. Easy assembly, fast and reliable signal and low consumption of the reagents make the system developed attractive for routine clinical analysis of metabolites.

Keywords: flow-through cell; chronoamperometry; uricase biosensor; ferrocene; pillarquinone; uricase determination; hydrogen peroxide determination

Citation: Stoikov, D.; Shafigullina, I.; Shurpik, D.; Stoikov, I.; Evtugyn, G. A Flow-Through Biosensor System Based on Pillar[3]Arene[2]Quinone and Ferrocene for Determination of Hydrogen Peroxide and Uric Acid. *Chemosensors* **2024**, *12*, 98. https://doi.org/10.3390/chemosensors12060098

Received: 30 April 2024
Revised: 21 May 2024
Accepted: 28 May 2024
Published: 4 June 2024

1. Introduction

Electrochemical enzyme biosensors are traditionally considered as very attractive in clinical analysis and environmental monitoring. They cover a large part of the commercial biosensor market [1]. Most such biosensors utilize immobilization of the enzymes on preliminary modified carriers to improve the biosensor performance and suppress interfering effects of the sample components [2]. An optimal matrix for enzyme immobilization provides a favorable microenvironment for the enzyme functioning and makes it possible to achieve necessary mechanical, thermal and chemical stability by preventing chemical and thermal enzyme denaturing [3]. This is particularly important for flow-through systems that show remarkable throughput of routine analysis in chemical laboratory and field conditions. Though the flow systems are less expensive in individual measurement than single-use sensors, they have undisputable advantages in mass analysis and screening investigations [4]. The development of simplified biosensing systems based on replaceable parts combined with portable measurement equipment can combine the strong points of conventional flow-through and single-use sensors.

To date, modified electrodes are mostly applied as signal transducers in electrochemical sensors. Modification can differentiate signals of the compounds with similar redox potentials, amplify recorded currents due to mediation of electron transfer, decrease the overvoltage of electrode reaction and accumulate the analyte molecules on the electrode interface [5].

Among many modifiers capable of improving sensor performance, macrocyclic compounds involved in specific interactions with the target species should be mentioned. Thus, substituted pillar[n]arenes both exert their own redox activity and form host–guest complexes with small molecules and ions [6]. Starting from 2008 [7], pillar[n]arene-based complexes have been intensively investigated to establish relationships between the host–guest complexation and properties of the guest molecules [8,9].

Pillar[n]arene consists of 1,4-hydroquinone units bonded by methylene bridges in the *para*-position. They can trap neutral organic molecules implemented in the microcavity by multiple non-covalent interactions [10]. In addition, they form hydrogen bonds between non-substituted hydroxyl groups and guest molecules and participate in the electrostatic interactions with participation of charged substituents of the macrocyclic core [11]. A variety of specific interactions and broad possibilities of chemical modification make pillar[n]arenes suitable for use in electrochemical sensors as adsorbents and mediators of electron transfer [12]. Previously, electrochemical sensors based on pillar[5]arene and its derivatives have been described for determination of paraquat [13], dopamine [14], bisphenol A [15], caffeic acid [16], tyramine, putrescine and cadaverine [17].

Uric acid (7,9-dihydro-1*H*-purine-2,6,8(3*H*)-trione) is a primary product of purine metabolism. Normally, it is present in urea on the level of 1.4 to 4.5 mM and in blood serum from 0.12 to 0.46 mM [18]. Changes in the uric acid concentration can be caused by abnormalities in purine exchange and by some illnesses, e.g., goat, hyperuricemia and Lesch–Nyhan syndrome [19,20]. A high concentration of uric acid can cause hypertension, urolithiasis and cardiovascular diseases.

Uric acid can be determined by a number of modern universal methods, e.g., spectrophotometry [21], fluorescence spectroscopy [22], gas chromatography [23] and high-performance liquid chromatography [24]. Being sensitive and selective, they offer high requirements for the sampling conditions, staff qualification and are rather expensive. Electrochemical non-enzymatic sensors show quite satisfactory results except high working potential and limited selectivity [25]. Some of these drawbacks can be overcome by implementation of nanomaterials able to increase the active surface of electrodes and diminish overvoltage of the reaction [26]. However, this makes the manufacture of the sensors more complicated and limits conditions of their operation.

Enzymatic determination of uric acid is mainly based on the use of uricase that catalyzes oxidation of the analyte by molecular oxygen to form hydrogen peroxide. The latter can be determined by the currents of its oxidation or reduction. Many modifiers including noble metal nanoparticles, carbon nanomaterials and transient metal complexes were successfully applied in the assembly of screen-printed electrodes (see recent reviews [27–30]). Although the results obtained allow the detection of very low concentrations of hydrogen peroxide, interest in the development of new mediator systems exists. Some of the recent results were presented in [31]. In the assembly of enzyme sensors, mediators of electron transfer mentioned are mostly combined with the species allowing covalent binding of uricase, e.g., zeolites, ion exchange polymers, carboxylated carriers, etc. [32–42]. As was already mentioned above, complex content and multistep deposition of the layer components complicates the manufacture of appropriate biosensors and is less compatible with the format of disposable biosensors for use outside chemical laboratories.

Previously, we have developed a biosensor system containing a replaceable enzyme reactor manufactured by 3D printing in combination with a screen-printed carbon electrode (SPCE) [43,44]. Here, the assembly of the reactor has been improved, and the volume of working cell decreased to 10 µL. For the first time, the SPCE modification was performed by carbon black, pillar[3]arene[2]quinone and ferrocene deposited from their suspension

in one step (one-pot synthesis). Pillar[3]arene[2]quinone and ferrocene exerted synergetic effect in the determination of hydrogen peroxide and showed an increase in the cathodic current against that recorded on similar electrodes modified with single components. This increased the sensitivity of H_2O_2 determination and allowed the detection of uricase activity based on the measurement of the quantities of hydrogen peroxide released in the enzymatic reaction of uric acid oxidation.

2. Materials and Methods

2.1. Reagents

Carbon black ENSACO 250G (CB, >99.95% C) was purchased from Imerys Graphite & Carbon (Willebroek, Belgium). Prior to use, 1.0 mg of carbon black was dispersed in 0.25 mL of concentrated nitric acid and 0.75 mL of concentrated sulfuric acid and sonicated for 60 min. Then, the sediment was centrifuged, washed and dried at 60 °C. Oxidized carbon black was suspended in 1.5 mL of propylene carbonate to its final concentration of 0.66 mg/mL.

Uricase from *Candida* sp. (EC 1.7.3.3, lyophilized powder, ≥2 units/mg solid, product No. U0880), uric acid, poly(lactic acid), ferrocene, *N*-(3-dimethylaminopropyl)-*N*′-ethylcarbodiimide chloride (EDC) and *N*-hydroxysuccinimide (NHS) were purchased from Sigma-Aldrich (St. Louis, MO, USA). Pillar[3]arene[2]quinone (Figure 1) was synthesized at the Department of Organic and Medicinal Chemistry of Kazan Federal University as described elsewhere [45].

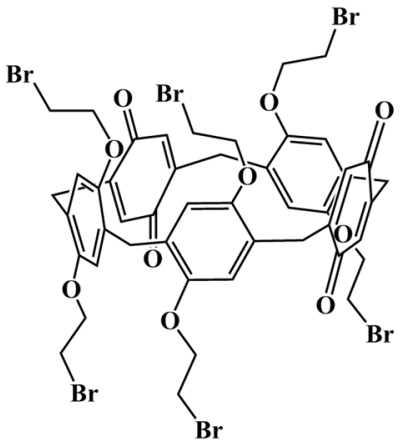

Figure 1. Chemical structure of pillar[3]arene[2]quinone used in the investigation.

All other reagents were of analytical grade. The solutions were prepared with deionized Millipore-Q water (Simplicity® water purification system, Merck-Millipore, Molsheim, France). Artificial urine consisted of 10 mM $CaCl_2$, 6 mM $MgCl_2$, 6 mM Na_2SO_4, 2 mM potassium citrate, 20 mM KH_2PO_4, 21 mM KCl, 18 mM NH_4Cl, 9 mM creatinine and 416 mM urea. Ringer–Locke solution mimicking plasma electrolytes contained 9.00 g/L NaCl, 0.42 g/L KCl, 0.25 g/L $CaCl_2$, 0.30 g/L $MgSO_4$, 0.50 rg/L $NaH_2PO_4 \cdot 2H_2O$ and 1.0 g/L glucose, pH 5.94.

Electrochemical measurements were performed in a 0.01 M phosphate buffer containing 0.1 M NaCl.

2.2. SPCE Modification

SPCEs were manufactured with the screen-printing instrument DEC 248 (DEK, London, UK) on Lomond PE DS Laser Film (thickness 125 μm, Lomond Trading Ltd., Douglas, Isle of Man) by consecutive printing of four layers, i.e., conducting silver tracks (polymeric silver paste PSP-2, Delta Paste, Moscow, Russia), pseudo-reference electrode (polymeric paste Ag/AgCl PSCP-1, Delta-Paste, Moscow, Russia), carbon tracks of auxiliary and working electrodes (carbon paste C2030519P4, Gwent Electronic Materials, Pontypool, UK) and

solvent-resistant blue dielectric paste D2140114D5 (Gwent Electronic Materials). Each layer was hardened at 80 °C. The geometric area of the working electrode was equal to 3.8 mm^2. Its modification was performed by drop-casting of 1 µL of suspension contained all three components, i.e., 0.66 mg/mL carbon black, 10 mM pillar[3]arene[2]quinone and 10 mM ferrocene in propylene carbonate. In the experiments performed with no ferrocene, the same volume and concentration of carbon black and of the macrocycle were used.

2.3. SEM Measurements

Scanning electron microscopy (SEM) images were recorded on the field emission scanning electron microscope Merlin™ (Zeiss, Jena, Germany).

2.4. Flow-through Cell Manufacture

The flow-through cell was manufactured using Wanhao Duplicator 9/300 (Jinhua Wanhao Spare Parts, Wanhao, Jinhua, China) equipped with an extruder (nozzle diameter 0.3 mm) made from poly(lactic acid) filaments. The material used is easily processed by 3D printing, is biodegradable, inexpensive and shows satisfactory accuracy of processing. The layer thickness was equal to 0.1 mm, with a printing rate of 700 mm/s and a printing temperature of 220 °C. The reactor consisted of two parts assembled with screws and flat washers. The assembled cell had the dimensions of 2.4 × 4.4 × 2.7 cm. A SPCE was fixed in the bottom part of the cell in a rectangular notch. The replaceable reactor contained two channels equipped with the plastic tubes with stainless steel needles for solution pumping. The reactor was placed in the rectangular notch in the upper part of the cell positions at 30° to ensure precise positioning of the reactor against the SPCE. All the reactions were conducted on the bottom of the reactor in the hollow with a depth of 0.6 mm and the square of 17 mm^2. The inner surface of the reactor walls was used for the enzyme immobilization. A schematic outline of the flow-through cell is presented in Figure 2.

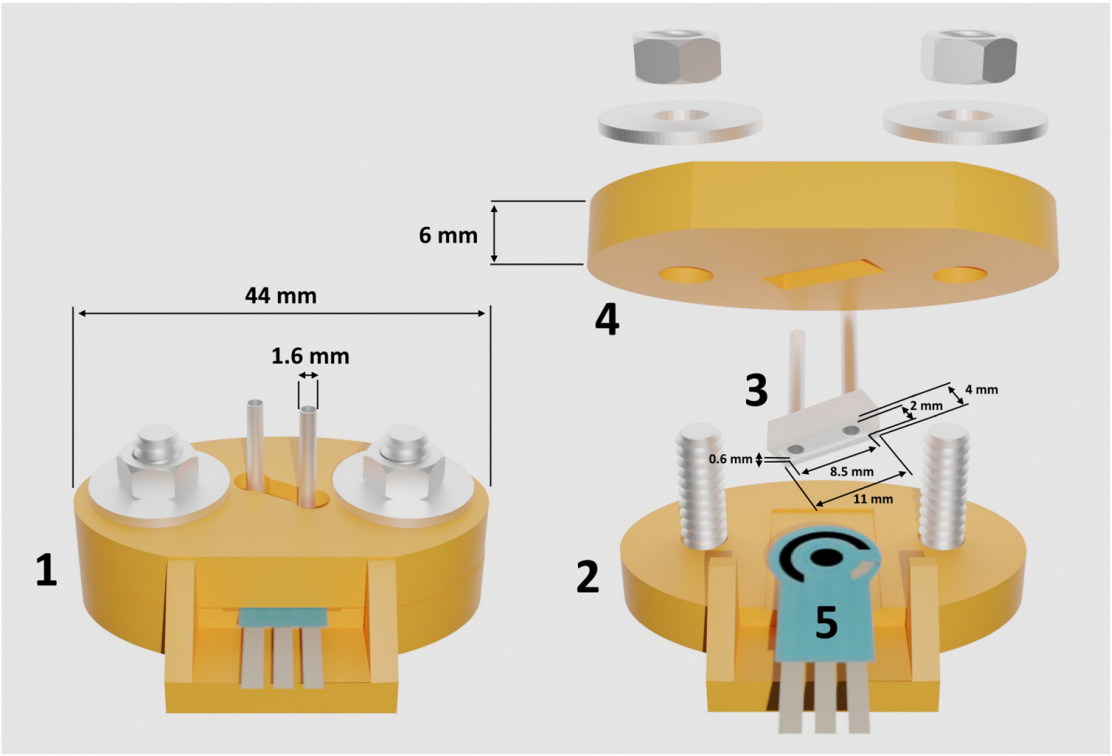

Figure 2. The assembly of flow-through cell. 1—cell assembled; 2—bottom part of the cell; 3—reactor; 4—upper part of the cell; 5—SPCE.

2.5. Enzyme Immobilization and Signal Measurement

For uricase immobilization, the reactor was fixed upside down. Then, 15 µL of 100 mM EDC was mixed with 15 µL of 400 mM NHS and drop-casted on the inner walls of the reactor. After 10 min of incubation, the reactor was washed with deionized water. After that, 15 µL of uricase solution was placed in the notch and allowed to dry at ambient temperature for 60 min. Immobilization was performed via terminal carboxylic groups of poly(lactic acid) and amino groups of the enzyme molecules by carbodiimide binding. Then, the reactor was gently washed out with working buffer and deionized water. The flow-through cell was assembled, and the solutions were pumped through the cell by a 100 Model syringe pump (ALS, Tokyo, Japan). The current of cathodic reduction of the hydrogen peroxide formed in the enzymatic reaction was recorded in chronoamperometric mode by a multichannel potentiostat (ESA Bioscience Inc., Chelmsford, MA, USA). Cyclic voltammograms in batch conditions were recorded with the CHI 440B potentiostat (CH Instruments Inc., Austin, TX, USA).

3. Results

3.1. Electrochemical Characterization of Pillar[3]Arene[2]–Ferrocene Coating

Pillar[5]arene has been successfully applied as mediator of electron transfer in electrochemical sensors [13–15]. Meanwhile, it was shown for perhydroxylated pillar[5]arene that it loses its activity during the sensor operation probably because of chemosorption of intermediate oxidation products. In addition, the voltammograms of pillar[5]arene are commonly complicated by intramolecular hydrogen bonding [46]. For this reason, quinone derivative of pillar[5]arene, i.e., pillar[3]arene[2]quinone, was selected for the SPCE modification. Preliminarily, it was shown that pillar[3]arene[2]quinone is capable of quasi-reversible reduction to hydroquinone derivative without the above-mentioned complications [45]. To some extent, the improvement of the macrocycle redox conversion can be attributed to the use of carbon nanomaterials that both enhance the working area and adsorb the macrocyclic mediator [6]. In this work, both components, i.e., carbon black and pillar[3]arene[2]quinone, were drop-casted on the electrode simultaneously from the same dispersion prepared in propylene carbonate. Earlier, pillar[5]arenes were dissolved in acetone and added to the surface layer after deposition of the carbon black. This resulted in irregular distribution of the mediator along the electrode square and complicated the protocol of electrode manufacture.

Figure 3 shows cyclic voltammograms recorded in batch conditions on the SPCE modified with pillar[3]arene[2]quinone and ferrocene. The quantities of the components were selected to reach full coverage of the electrode. They corresponded to the 1:1 stoichiometry of ferrocene inclusion in the pillar[5]arene moiety. New oxidation peaks (0.272 V for pillar[3]arene[2]quinone and 0.292 V for its mixture with ferrocene) and reduction peaks (−0.368 V for pillar[3]arene[2]quinone and −0.298 V for its mixture with ferrocene) appeared on the voltammograms.

The use of electrochemical impedance spectroscopy for monitoring of the surface-layer assembly is complicated by the common area of redox activity of the $[Fe(CN)_6]^{3-/4-}$ redox pair used as a redox probe and pillar[3]arene[2]quinone placed on the electrode interface.

The conditions of the signal measurements were similar to those previously applied in flow-through amperometric biosensors with uricase and acetylcholinesterase utilizing pillararene mediators. The electrochemistry of pillar[3]arene[2]quinone was intensively investigated in [45]. As was shown for the macrocycle both dissolved in aqueous solution and adsorbed on carbon black, the reduction of quinone fragments is significantly influenced by neighboring substituents of the pillararene rings. This was the reason to introduce ferrocene as an auxiliary mediator of electron transfer.

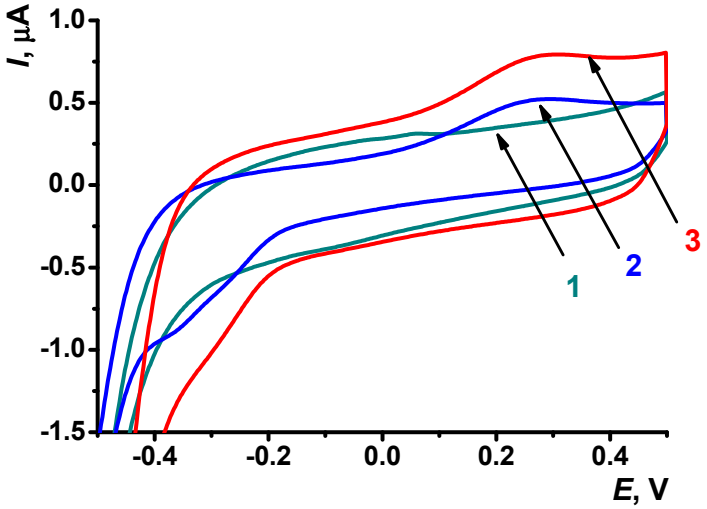

Figure 3. Cyclic voltammograms recorded on a SPCE modified with carbon black and ferrocene (1), pillar[3]arene[2]quinone (2) and their mixture (3); 0.01 M phosphate buffer + 0.1 M NaCl, scan rate 100 mV/s.

Ferrocene is stable in the measurement conditions including the pH changes. In addition, the electron transfer in the ferrocene/ferricenium redox pair does not assume structural changes so that the overvoltage of appropriate reaction is low. All of this makes ferrocene an effective mediator of electron transfer. Nevertheless, the electrode modified with ferrocene incorporated alone in the carbon black showed only a very small and broad oxidation peak at 0.1 V, which did not significantly change with the quantities of ferrocene introduced. This might result from incorporation of the ferrocene molecules in the pores of carbon black and their separation from the electrode interface by propylene carbonate film. Previously, it was demonstrated that ferrocene is deeply entrapped in the particles of carbon black [47]. The addition of pillar[5]arene[2]quinone shifted the equilibrium of ferrocene adsorption toward the host–guest complex similarly to that described in the literature [48]. This would result in an increase in the redox currents attributed to the macrocycle even though no separate peaks of ferrocene redox conversion appeared on the voltammograms.

3.2. SEM Investigation

Deposition of carbon black on the SPCE results in the formation of a regular layer with roundish carbon particles evenly distributed along the working surface (Figure 4a). The drop-casting of the mixture consisted of carbon black and pillar[3]arene[2]quinone, resulting in the formation of a thin film, which partially masks the underlying carbon black particles and contains rather big pores and hollows on the filled parts of the electrode. They could probably be attributed to the molecular aggregates of the macrocycle/ferrocene complexes that are located on more hydrophobic molecular layers of the components. The morphology of the coating did not depend on the addition of ferrocene and was similar to that previously reported for the coating of pillar[3]arene[2]quinone on glassy carbon electrode modified with carbon black for the same loading of modifiers [45]. It can be concluded that modification with carbon black eliminates the possible difference between the SPCE and glassy carbon as primary transducers.

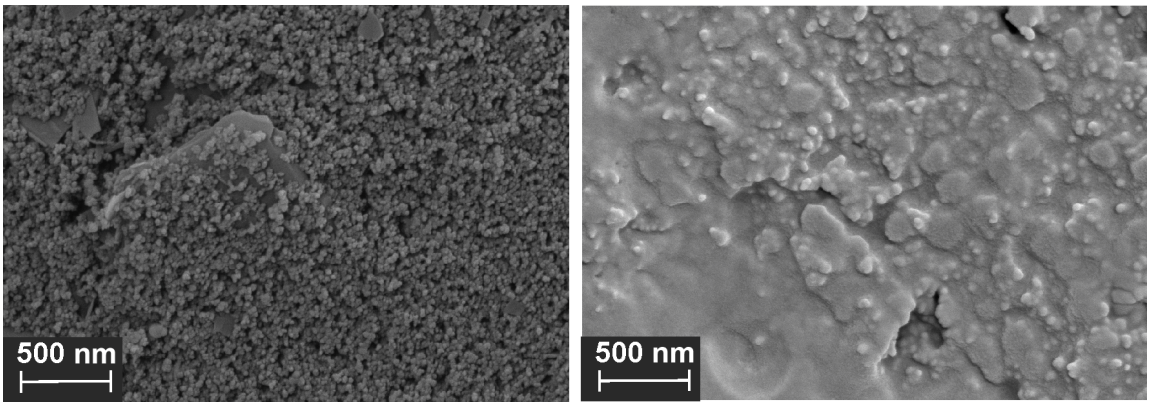

(**a**) (**b**)

Figure 4. SEM images of the SPCE covered with carbon black deposited from propylene carbonate suspension (**a**) and with 10 mM pillar[3]arene[2]quinone mixed with equimolar ferrocene quantities and suspended with carbon black in propylene carbonate (**b**).

3.3. Hydrogen Peroxide Determination

H_2O_2 is commonly formed in the reactions catalyzed by oxidoreductases. Thus, its detection by appropriate sensors makes it possible to determine organic substrates of such enzymatic reactions. Although hydrogen peroxide can be oxidized on the electrode, cathodic reduction has some advantages related to less interference with common species present in biological fluids, e.g., ascorbic acid or paracetamol.

Indeed, switching the flow from the phosphate buffer to that with dissolved H_2O_2 resulted in generation of cathodic current attributed to the reduction of hydrogen peroxide. Figure 5 shows the dependence of the maximal shift of the current recorded in chronoamperometric mode after the H_2O_2 addition on the working potential and flow rate. The results were obtained for 10 µM H_2O_2 flow.

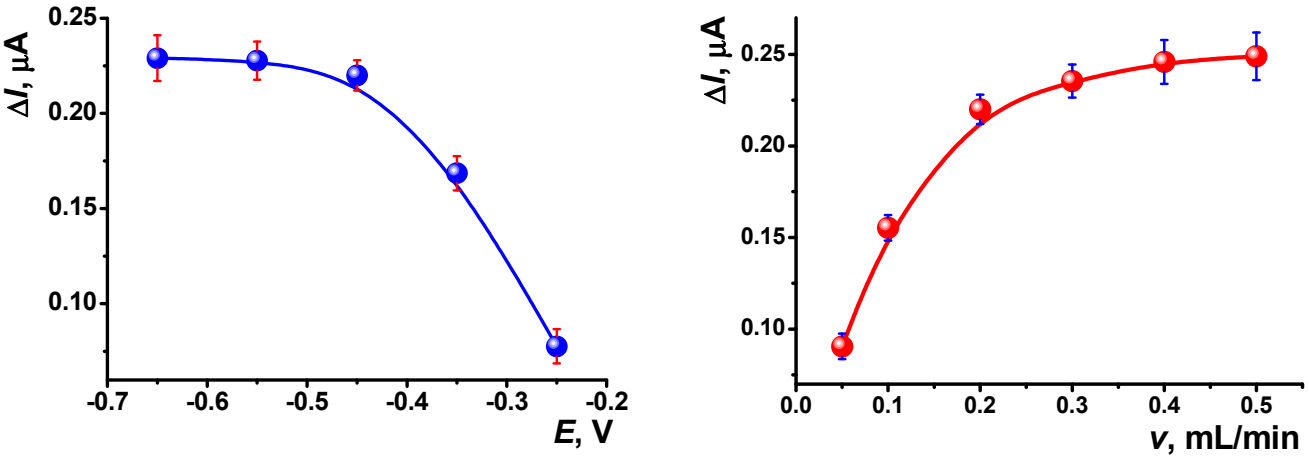

(**a**) (**b**)

Figure 5. The dependence of the maximal current shift (average ± S.D. for five individual SPCEs modified with pillar[3]arene[2]quinone and ferrocene) reached after the addition of 10 µM H_2O_2 in the flow of 0.01 M phosphate buffer containing 0.1 M NaCl on the (**a**) working potential and (**b**) flow rate.

The signal increased with the flow rate until 0.2 mL/min and was maximal at the potential of 0.45 V. All the following experiments were performed at this working potential. Simultaneous application of two mediators, i.e., pillar[3]arene[2]quinone and ferrocene,

increased the maximal current shift about fivefold against that reached for individual mediators.

Dynamic response to H_2O_2 obtained by switching the flows of the phosphate buffer and H_2O_2 solution is shown in Figure 6a, and calibration curves of H_2O_2 obtained with variously modified SPCEs in Figure 6b. One can see that changes in the cathodic currents followed the switching of the flows and were reversible. Implementation of pillar[3]arene[2]quinone/ferrocene significantly increased maximal shift in the current. The dynamic changes in the current corresponding to this coating are presented in Figure 6c to demonstrate the high stability of the background current. Maximal shifts in the current were used for calibration curve 3 present in Figure 6b.

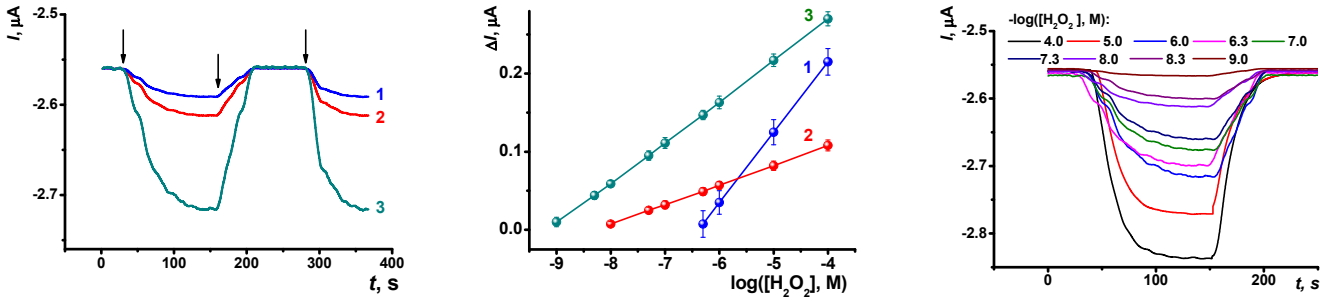

Figure 6. (**a**) Dynamic response to the 10 μM H_2O_2 recorded in chronoamperometric mode by flow switching with the SPCE modified with ferrocene (1), pillar[3]arene[2]quinone (2) and their mixture (3). Arrows indicate switching the flows from phosphate buffer to that with hydrogen peroxide and back. (**b**) Calibration curves of H_2O_2 determination. Average ± S.D. for five individual electrodes is presented for the maximal current shifts recorded. (**c**) Dynamic response toward various concentrations of hydrogen peroxide obtained with the SPCE modified with pillar[3]arene[2]quinone/ferrocene.

Analytical characteristics of hydrogen peroxide determination are summarized in Table 1. The limit of detection (LOD) was calculated as $3x/y$, where x is the standard deviation (S.D.) of the background current and y is the slope of the calibration curve; n is the number of experimental points within a linear piece of the plot.

Table 1. Analytical characteristics of the hydrogen peroxide determination with the flow-through system and modified SPCEs.

Modifier	$\Delta(I, \mu A) = a + b \times \log(c, M)$ a	b	R^2	n	Concentration Range, $-\log(c, M)$	LOD, nM
Ferrocene	0.5775 ± 0.0006	0.0901 ± 0.0001	0.9999	4	6.5–4	6000
Pillar[3]arene[2]quinone	0.207 ± 0.001	0.0249 ± 0.001	0.9998	7	8–4	40
Pillar[3]arene[2]quinone + ferrocene	0.476 ± 0.001	0.0520 ± 0.0003	0.9997	9	9–4	0.3

The response time assessed for 20 consecutive switches of the flow was 3 min. No significant drifts of the currents were observed within this time period. In continuous flow, the steady-state current recorded in the absence of hydrogen peroxide during one hour changed by not more than 0.05 μA (ambient temperature) and in the presence of 10 μM H_2O_2 by 0.15 μA. It should be also noted that switching the flows from the buffer to that with H_2O_2 and back resulted in recovery of the background current with its deviation by 0.1 μA (20 consecutive measurements). This did not significantly affect the response (current shift toward a constant H_2O_2 concentration), which was more reproducible than the absolute current value. The measurement-to-measurement repeatability of the currents shifts was found to be 2.5% and 5.5% for five individual sensors modified with the same set of reagents. Storage of the modified SPCEs in dry conditions for one hour increased the

deviation of the current shifts to 5.5 and 0.5% (measurement-to-measurement and sensor-to-sensor repeatability, respectively). In the working buffer, the lifetime of the modification layer assessed as the period of 50% decay of the response toward 10 μM H_2O_2 was equal to three days at ambient temperature and one weak at 4 °C.

The addition of ferrocene to the macrocycle in the surface layer resulted in an extension of the linear piece of calibration curve and an approximately twofold increase in the slope against pillar[3]arene[2]quinone taken alone. This can be explained by implementation of the ferrocene in the electron transfer path and by partial suppression of steric hindrance of direct cathodic reduction of quinone units in the macrocycle. Ferrocene alone proved its reputation as an excellent mediator of electron transfer. It showed the maximal slope of the calibration curve among the modifiers considered. Meanwhile, it should be noted that the S.D. of the ferrocene signal was also two times higher than that for the coatings containing the macrocycle. In addition, the concentration range reached for ferrocene-mediated reduction of hydrogen peroxide was quite narrow.

Table 2 contains the comparison of the analytical characteristics of H_2O_2 determination achieved with electrochemical sensors reported in the literature. We realize that the determination of hydrogen peroxide is one of the most common subjects of electrochemical sensor development, and the number of appropriate sensors is very high. In Table 2, some typical examples of the approaches to the surface-layer assembly and appropriate characteristics of H_2O_2 determination are summarized.

Table 2. Comparison of the electrochemical characteristics of the sensors developed with other electrochemical sensors for hydrogen peroxide determination described in the literature.

Electrode/Modifier	Detection Mode	Concentration Range, M	LOD, M	Ref.
Au/chitosan	Cyclic voltammetry	8×10^{-7}–1.3×10^{-2}	9.8×10^{-7}	[49]
Glassy carbon electrode/Cu_2O/polyaniline/reduced graphene oxide	Chronoamperometry	8.5×10^{-4}–12.78×10^{-2}	5×10^{-7}	[50]
Carbon-paste electrode/surfactant/carbon–maghemite composite	Cyclic voltammetry	1×10^{-5}–1.5×10^{-3}	2.78×10^{-6}	[51]
Glassy carbon electrode/MoS_2/graphene oxide	Cyclic voltammetry	1×10^{-5}–5.57×10^{-3}	1.9×10^{-6}	[52]
Pillar[3]arene[2]quinone/carbon black	Chronoamperometry	1×10^{-8}–1×10^{-4}	5×10^{-9}	This work
Pillar[3]arene[2]quinone/ferrocene/carbon black	Chronoamperometry	1×10^{-9}–1×10^{-4}	3×10^{-10}	This work

The electrochemical determination of H_2O_2 was validated with commercial samples of disinfectants purchased in the local market. They contained 0.18–0.25 M H_2O_2 and some additives (emulsifiers, stabilizers, odorants, colorants, etc.). The hydrogen peroxide content of the samples was independently determined by titration with potassium permanganate. Prior to determination, disinfectants were diluted with working phosphate buffer in the ratio of 1:1000 to $1:10^9$. Appropriate calibration curves and accuracy assessed by the "Added–Found" method are presented in Figure S1 and Table S1 (Electronic Supporting Information). In them, the H_2O_2 concentrations calculated after the dilution were used. One can see the slopes of the curves have not significantly changed against that of H_2O_2 standard solution. The recovery rates varied from 85 to 114%. Thus, electrochemical flow-through sensors can be applied for H_2O_2 determination in a wide range of its concentrations.

3.4. Biosensor System for Uric Acid Determination

For immobilization of uric acid, carbodiimide binding was specified as one of the most reliable techniques for covalent immobilization of biomolecules via formation of amide bonds between terminal carboxylic and primary amino groups. Here, carboxylic groups of poly(lactic) acid used for the manufacture of flow-through reactors were consecutively treated with EDC and NHS to "activate" the inner surface of the polymer. Then, uricase

solution was added. The reactions of the enzyme immobilization are presented in Scheme 1. The immobilization protocol was elaborated and successfully applied in our previous work [43] and used here without modification.

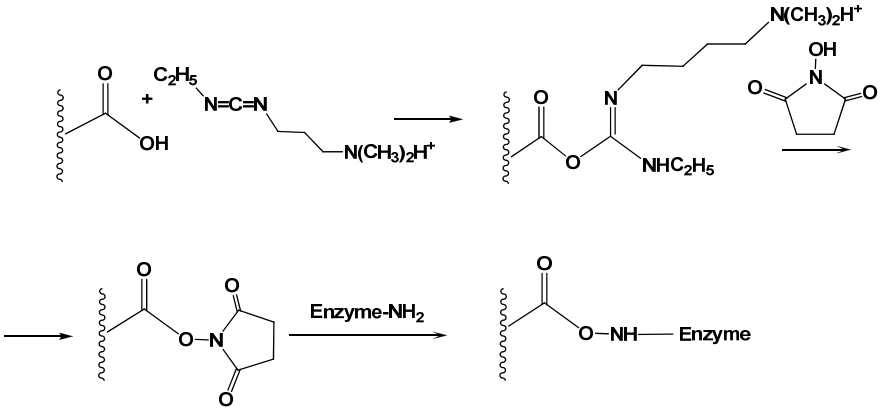

Scheme 1. Carbodiimide binding of uricase.

In the presence of uric acid, the immobilized enzyme catalyzes its oxidation with the formation of hydrogen peroxide (2) (Scheme 2).

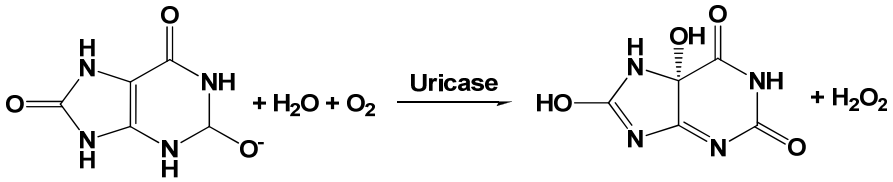

Scheme 2. Enzymatic reaction of uric acid oxidation.

It is moved to the working electrode and cathodically reduced. The current recorded in chronoamperometric mode increased with the uric acid concentration. The amounts of the enzyme and working pH were selected to reach the maximal and most reproducible response. Thus, with the deposition of 1.0–5.0 U of uricase per reactor, the maximal signal toward 10 μM of uric acid was obtained for 2.0 U of enzyme. The pH dependence of the response was investigated by a stepwise shift of the buffer pH that was passed through the reactor. The signal increased as the pH changed from 7.0 to 9.0. This corresponded to the pH dependence of native uricase [53]. The biosensor system with the SPCE modified with pillar[3]arene[2]quinone in the carbon black layer made it possible to determine from 0.05 to 10 μM uric acid (LOD 0.02 μM). The addition of ferrocene improved the biosensor performance. The linear range of concentrations determined covered 0.01–10 μM with a LOD of 0.01 μM. Appropriate calibration curves are presented in Figure S2. The biosensor system makes it possible to perform 20 measurements per hour and can be continuously used for at least 8 h without any losses of enzyme activity and signal sensitivity toward the uric acid.

Analytical characteristics of uric acid determination achieved with the biosensor system developed are comparable with those reported for other electrochemical sensors and biosensors (Table 3).

Table 3. Comparison of the analytical characteristics of the sensors and biosensors for uric acid determination described in the literature.

Modifier	Detection Mode	Concentration Range, M	LOD, M	Ref.
Polypyrrole, graphene, Pt nanoparticles	CV	2×10^{-9}–2.4×10^{-8}	5.41×10^{-10}	[32]
Horseradish peroxidase, Au nanoparticles, multiwalled carbon nanotubes	CV	5×10^{-5}–6.5×10^{-4}	9.91×10^{-6}	[33]
Graphene oxide	DPV	2×10^{-5}–4.9×10^{-4}	3.45×10^{-6}	[34]
Cu_2ZnSnS_4	DPV	5×10^{-8}–7×10^{-4}	6.6×10^{-8}	[35]
Nafion, ZnO nanorods	CV	1×10^{-3}–1×10^{-2}	2.3×10^{-5}	[36]
Au/reduced graphene oxide	DPV	5×10^{-5}–8×10^{-4}	5.32×10^{-6}	[37]
N-doped graphene aerogel	CV	4×10^{-7}–5×10^{-5}	1.2×10^{-7}	[38]
Carbon nanotubes, carboxymethylcellulose	CV	2×10^{-5}–2.7×10^{-3}	2.8×10^{-6}	[39]
Zeolite imidazolate framework-11	DPV	5×10^{-6}–5.4×10^{-4}	4.8×10^{-7}	[40]
Magnetite decorated urchin-like *N*-doped carbon	DPV	2×10^{-6}–2×10^{-4}	2.9×10^{-7}	[41]
Covalent organic framework and multiwalled carbon nanotubes with Co nanoparticles	DPV	6×10^{-7}–2.5×10^{-4}	6.3×10^{-8}	[42]
Uricase on reactor, pillar[3]arene[2]quinone in carbon black layer	CA	5×10^{-8}–1×10^{-5}	2×10^{-8}	This work
Uricase on reactor, pillar[3]arene[2]quinone/ferrocene in carbon black layer	CA	1×10^{-8}–1×10^{-5}	1×10^{-8}	This work

CA—chronoamperometry, CV—cyclic voltammetry, DPV—differential-pulse voltammetry.

It should be noted that application of the uricase biosensors in medical diagnostics assumes measurement of much higher levels of uric acid so that multiple dilution of the samples is required. On the other hand, such a dilution allows avoiding possible interference caused by the components on biological fluids.

The precision of the measurement of the signal toward uric acid was assessed in five consecutive measurements with the same replaceable reactor and SPCE modified with pillar[3]arene[2]quinone. The standard deviation of the current shift was found to be 3.2% for 10 μM uric acid, or 1.5 times bigger than that of the hydrogen peroxide determination. Similar experiments with five replaceable reactors and five individual electrodes increased the S.D. to 7.7%. No significant alterations of the signal were observed in continuous flow of the uric acid within at least 8 h. In dry conditions, 50% of initial enzyme activity was reached after four months of storage in dry conditions with freshly prepared modified SPCE.

Oxidizable species did not affect the signal toward uric acid. The following potential interferences were tested. In brackets, maximal no-effect concentrations are mentioned: glucose (50 μM), dopamine (0.5 mM), paracetamol (1 mM), tyrosine (1 mM) and ascorbic acid (50 μM). The electrolyte content of blood plasma was mimicked by the Ringer–Locke solution (the content is presented in Materials and Methods). The recovery rate for 10 μM uric acid was equal to 96% (five repetitions). In artificial urine (content is present in Materials and Methods), a recovery rate of 115% was found in the undiluted sample and 102% for threefold-diluted artificial urine. Determination results are presented in Table S2.

4. Conclusions

A flow-through enzymatic system with uricase immobilized on the inner walls of a replaceable reactor was manufactured from poly(lactic acid) by 3D printing. In comparison with the previously described assembly [43], the following improvements were introduced. The new geometry of the reactor decreased the volume of the working cell to 10 μL. The rectangular shape of the reactor increased the laminarity of the flow and diminished interferences with the amperometric signal measurement. Contrary to conventional flow-through systems, the SPCE modified with the macrocycle, and ferrocene was spatially separated from the immobilized enzyme. This made it possible to select the electrode modification and enzyme immobilization protocols separately from each other. Deposition

of pillar[3]arene[2]quinone and ferrocene together with the carbon black suspension in a single step also showed advantages over the traditional step-by-step protocol. The "one-pot synthesis" simplified and made the manufacture of the modified electrodes more reliable and demonstrated high durability of the surface coating in continuous flow. The flow-through system was first tested on the determination of hydrogen peroxide, which is a common target in enzyme sensors with immobilized oxidoreductases. It was rather surprising to find a wider range of H_2O_2 concentrations detected and higher currents recorded against those of a similar system utilizing only pillar[3]arene[2]quinone without ferrocene. This might result from the implementation of ferrocene in the electron transfer by its implementation in the macrocycle cavity. This would partially suppress steric hindrance of the access of quinone fragments to the electrode interface. To some extent, lower signals of ferrocene/ferricenium redox conversion found on the carbon black layer can be also attributed to the use of propylene carbonate as a film-forming agent and solvent required in modification. It provided solubility of all the modifiers used in comparison with previously applied acetone or acetonitrile. The determination of hydrogen peroxide was proven on the example of disinfectant analysis, which showed a high recovery rate and precision of the measurement.

After that, the developed flow-through biosensor system was applied for the determination of uric acid, a substrate of uricase and metabolite demanded in medical diagnostics of some diseases. The characteristics of uric acid determination, including a LOD of 0.3 nM, were better than those achieved in the absence of ferrocene in the surface layer and comparable with other electrochemical biosensors described in the literature. The flow-through biosensor system allowed up to 20 measurement per hour to be conducted with no drift of the signal within a working day. Considering the simple replacement of the enzyme reactor, the low cost of its production by 3D printing from poly(lactic acid) filaments and the mild requirements for the labor staff and sample treatment, the system developed is attractive for the use in medicine in the point-of-care testing format. The low flow rates and minimal quantities of the reagents required for the manufacture of the biosensor system as well as broad possibilities of its adaption to other oxidoreductases make it possible to conclude that such devices have promising prospects in routing medical analysis.

Supplementary Materials: The following supporting information can be downloaded at: https://www.mdpi.com/article/10.3390/chemosensors12060098/s1, Figure S1: H_2O_2 calibration curves obtained with a flow-through system with a SPCE modified with pillar[3]arene[2]quinone and ferrocene in the layer of carbon black; Figure S2: Calibration curves of uric acid on a SPCE modified with pillar[3]arene[2]quinone and ferrocene; Table S1: Accuracy of chronoamperometric determination of 10 μM hydrogen peroxide in diluted commercial disinfectants; Table S2: Chronoamperometric determination of uric acid in artificial urine and Ringer–Locke solution.

Author Contributions: Conceptualization, G.E. and I.S. (Ivan Stoikov); methodology, G.E., D.S. (Dmitry Shurpik) and I.S. (Ivan Stoikov); validation, I.S. (Insiya Shafigullina) and D.S. (Dmitry Shurpik); formal analysis, D.S. (Dmitry Stoikov) and I.S. (Insiya Shafigullina); investigation, D.S. (Dmitry Stoikov), D.S. (Dmitry Shurpik) and I.S. (Insiya Shafigullina); resources, D.S. (Dmitry Shurpik) and I.S. (Ivan Stoikov); data curation, G.E. and I.S. (Ivan Stoikov); writing—original draft preparation, G.E. and D.S. (Dmitry Stoikov); visualization, D.S. (Dmitry Stoikov) and D.S. (Dmitry Shurpik); supervision, G.E. and I.S. (Ivan Stoikov); project administration, G.E. and I.S. (Ivan Stoikov); funding acquisition, G.E. All authors have read and agreed to the published version of the manuscript.

Funding: This research was funded by the Russian Science Foundation, Project Number 22-13-00070.

Institutional Review Board Statement: Not applicable.

Informed Consent Statement: Not applicable.

Data Availability Statement: Data are contained within the article and Supplementary Materials.

Conflicts of Interest: The authors declare no conflicts of interest.

References

1. Bucur, B.; Purcarea, C.; Andreescu, S.; Vasilescu, A. Addressing the selectivity of enzyme biosensors: Solutions and perspectives. *Sensors* **2021**, *21*, 3038. [CrossRef]
2. Yamaguchi, H.; Miyazaki, M. Enzyme-immobilized microfluidic devices for biomolecule detection. *TrAC—Trend Anal. Chem.* **2023**, *159*, 116908. [CrossRef]
3. Sheldon, R.A.; van Pelt, S. Enzyme immobilisation in biocatalysis: Why, what and how. *Chem. Soc. Rev.* **2013**, *42*, 6223–6235. [CrossRef]
4. Sahragard, A.; Varanusupakul, P.; Miró, M. Nanomaterial decorated electrodes in flow-through electrochemical sensing of environmental pollutants: A critical review. *Trends Environ. Anal. Chem.* **2023**, *39*, e00208. [CrossRef]
5. Yang, X.; Liu, C.; Chen, Z. Rapid determination of uric acid in human urine by CE with an improved electromagnetic induction detector. *Chromatographia* **2014**, *78*, 119–123. [CrossRef]
6. Smolko, V.A.; Shurpik, D.N.; Shamagsumova, R.V.; Porfireva, A.V.; Evtugyn, V.G.; Yakimova, L.S.; Stoikov, I.I.; Evtugyn, G.A. Electrochemical behavior of pillar[5] on glassy carbon electrode and its interaction with Cu^{2+} and Ag^{+} ions. *Electrochim. Acta* **2014**, *147*, 726–734. [CrossRef]
7. Ogoshi, T.; Kanai, S.; Fujinami, S.; Yamagishi, T.; Nakamoto, Y. Para-bridged symmetrical pillar[5]arenes: Their Lewis acid catalyzed synthesis and host–guest property. *J. Am. Chem. Soc.* **2008**, *130*, 5022–5023. [CrossRef]
8. Ogoshi, T.; Yamagishi, T.; Nakamoto, Y. Pillar-shaped macrocyclic hosts pillar[n]arenes: New key players for supramolecular chemistry. *Chem. Rev.* **2016**, *116*, 7937–8002. [CrossRef]
9. Wang, Y.; Ping, G.; Li, C. Efficient complexation between pillar[5]arenes and neutral guests: From host–guest chemistry to functional materials. *Chem. Commun.* **2016**, *52*, 9858–9872. [CrossRef]
10. Ohtani, S.; Kato, K.; Fa, S.; Ogoshi, T. Host–guest chemistry based on solid-state pillar[n]arenes. *Coord. Chem. Rev.* **2022**, *462*, 214503. [CrossRef]
11. Xia, W.; Hu, X.Y.; Chen, Y.; Lin, C.; Wang, L. A novel redox-responsive pillar[6]arene-based inclusion complex with a ferrocenium guest. *Chem. Commun.* **2013**, *49*, 5085–5087. [CrossRef]
12. Acikbas, Y.; Aksoy, M.; Aksoy, M.; Karaagac, D.; Bastug, E.; Kursunlu, A.N.; Erdogan, M.; Capan, R.; Ozmen, M.; Ersoz, M. Recent progress in pillar[n]arene-based thin films on chemical sensor applications. *J. Incl. Phenom. Macrocycl. Chem.* **2021**, *100*, 39–54. [CrossRef]
13. Sun, J.; Guo, F.; Shi, Q.; Wu, H.; Sun, Y.; Chen, M.; Diao, G. Electrochemical detection of paraquat based on silver nanoparticles/water-soluble pillar[5]arene functionalized graphene oxide modified glassy carbon electrode. *J. Electroanal. Chem.* **2019**, *847*, 113221. [CrossRef]
14. Tan, X.; He, S.; Liu, X.; Zhao, G.; Huang, T.; Yang, L. Ultrasensitive electrochemical sensing of dopamine by using dihydroxylatopillar[5]arene-modified gold nanoparticles and anionic pillar[5]arene-functionalized graphitic carbon nitride. *Microchim. Acta* **2019**, *186*, 703. [CrossRef]
15. Liang, H.; Zhao, Y.; Ye, H.; Li, C.-P. Ultrasensitive and ultrawide range electrochemical determination of bisphenol A based on PtPd bimetallic nanoparticles and cationic pillar[5]arene decorated graphene. *J. Electroanal. Chem.* **2019**, *855*, 113487. [CrossRef]
16. Wang, J.; Zhou, L.; Bei, J.; Zhao, Q.; Li, X.; He, J.; Cai, Y.; Chen, T.; Du, Y.; Yao, Y. An enhanced photo-electrochemical sensor constructed from pillar[5]arene functionalized Au NPs for ultrasensitive detection of caffeic acid. *Talanta* **2022**, *243*, 123322. [CrossRef]
17. Erdogan, Z.O.; Kursunlu, A.; Kucukkolbasi, S. Pillar[5]arene based non-enzymatic and enzymatic tyramine sensor. *IEEE Sens. J.* **2021**, *21*, 5728–5735. [CrossRef]
18. Pachla, L.A.; Reynolds, D.L.; Wright, D.S.; Kissinger, P.T. Analytical methods for measuring uric acid in biological samples and food products. *J. AOAC Int.* **1987**, *70*, 1–14. [CrossRef]
19. Ullman, B.; Wormsted, M.A.; Cohen, M.B.; Martin, D.W. Purine oversecretion in cultured murine lymphoma cells deficient in adenylosuccinate synthetase: Genetic model for inherited hyperuricemia and gout. *Proc. Natl. Acad. Sci. USA* **1982**, *79*, 5127–5131. [CrossRef]
20. Yamanaka, H.; Togashi, R.; Hakoda, M.; Terai, C.; Kashiwazaki, S.; Dan, T.; Kamatani, N. Optimal range of serum urate concentrations to minimize risk of gouty attacks during anti-hyperuricemic treatment. *Purine Pyrimidine Met.* **1998**, *431*, 13–18. [CrossRef]
21. Rocha, D.L.; Rocha, F.R.P. A flow-based procedure with solenoid micro-pumps for the spectrophotometric determination of uric acid in urine. *Microchem. J.* **2010**, *94*, 53–59. [CrossRef]
22. Jin, D.; Seo, M.-H.; Huy, B.T.; Pham, Q.-T.; Conte, M.L.; Thangadurai, D.; Lee, Y.I. Quantitative determination of uric acid using CdTe nanoparticles as fluorescence probes. *Biosens. Bioelectron.* **2016**, *7*, 359–365. [CrossRef] [PubMed]
23. Zhang, Y.; Jin, H.; Li, X.; Zhao, J.; Guo, X.; Wang, J.; Liang, X. Separation and characterization of bufadienolides in toad skin using two-dimensional normal-phase liquid chromatography × reversed-phase liquid chromatography coupled with mass spectrometry. *J. Chromatogr. B* **2016**, *1026*, 67–74. [CrossRef] [PubMed]
24. Dai, H.; Wang, N.; Wang, D.; Zhang, X.; Ma, H.; Lin, M. Voltammetric uric acid sensor based on a glassy carbon electrode modified with a nanocomposite consisting of polytetraphenylporphyrin, polypyrrole, and graphene oxide. *Microchim. Acta* **2016**, *183*, 3053–3059. [CrossRef]

25. Hernández-Ramírez, D.; Mendoza-Huizar, L.H.; Galán-Vidal, C.A.; Aguilar-Lira, G.Y.; Álvarez-Romero, G.A. Review—Trends on the development of non-enzymatic electrochemical sensors modified with metal-oxide nanostructures for the quantification of uric acid. *J. Electrochem. Soc.* **2021**, *168*, 057522. [CrossRef]
26. Beitollahi, H.; Movahedifar, F.; Tajik, S.; Jahani, S. A Review on the effects of introducing CNTs in the modification process of electrochemical sensors. *Electroanalysis* **2018**, *31*, 1195–1203. [CrossRef]
27. Antuña-Jiménez, D.; González-García, M.B.; Hernández-Santos, D.; Fanjul-Bolado, P. Screen-printed electrodes modified with metal nanoparticles for small molecule sensing. *Biosensors* **2020**, *10*, 9. [CrossRef] [PubMed]
28. Silva, R.M.; da Silva, A.D.; Camargo, J.R.; de Castro, B.S.; Meireles, L.M.; Silva, P.S.; Janegitz, P.C.; Silva, T.A. Carbon nanomaterials-based screen-printed electrodes for sensing applications. *Biosensors* **2023**, *13*, 453. [CrossRef] [PubMed]
29. Komkova, M.; Karyakin, A. Prussian blue: From advanced electrocatalyst to nanozymes defeating natural enzyme. *Microchim. Acta* **2022**, *189*, 290. [CrossRef]
30. Xing, L.; Zhang, W.; Fu, L.; Lorenzo, J.M.; Hao, Y. Fabrication and application of electrochemical sensor for analyzing hydrogen peroxide in food system and biological samples. *Food Chem.* **2022**, *385*, 132555. [CrossRef]
31. Zribi, R.; Ferlazzo, A.; Fazio, E.; Condorelli, M.; D'Urso, L.; Neri, G.; Corsaro, C.; Neri, F.; Compagnini, G.; Neri, G. Ag nanoplates modified-screen printed carbon electrode to improve electrochemical performances. Toward a selective H_2O_2 detection. *IEEE Trans. Instrum. Meas.* **2023**, *72*, 6002708. [CrossRef]
32. Giarola, J.F.; Mano, V.; Pereira, C. Development and application of a voltammetric biosensor based on polypyrrole/uricase/graphene for uric acid determination. *Electroanalysis* **2018**, *30*, 119–127. [CrossRef]
33. Bhushan, P.Y.; Umasankar, S.R.; Choudhury, P.A.; Hirt, F.E.; Mac Quhaec, L.J.; Borda, H.A.; Lev-Tov, R.S.; Kirsner, R.S.; Bansali, S. Biosensor for monitoring uric acid in wound and its proximity: A potential wound diagnostic tool. *J. Electrochem. Soc.* **2019**, *166*, B830–B836. [CrossRef]
34. Omar, M.N.; Salleh, A.B.; Lim, H.N.; Tajudin, A.A. Electrochemical detection of uric acid via uricase-immobilized graphene oxide. *Anal. Biochem.* **2016**, *509*, 135–141. [CrossRef] [PubMed]
35. Jain, S.; Verma, S.; Singh, S.P.; Sharma, S.N. An electrochemical biosensor based on novel butylamine capped CZTS nanoparticles immobilized by uricase for uric acid detection. *Biosens. Bioelectron.* **2019**, *127*, 135–141. [CrossRef] [PubMed]
36. Ahmad, R.N.; Tripathy, N.; Ahn, M.-S.; Hahn, Y.-B. Solution process synthesis of high aspect ratio ZnO nanorods on electrode surface for sensitive electrochemical detection of uric acid. *Sci. Rep.* **2017**, *7*, 46475. [CrossRef]
37. Verma, S.; Choudhary, J.; Singh, K.P.; Chandra, P.; Singh, S.P. Uricase grafted nanoconducting matrix based electrochemical biosensor for ultrafast uric acid detection in human serum samples. *Int. J. Biol. Macromol.* **2019**, *130*, 333–341. [CrossRef]
38. Feng, S.; Yu, L.; Yan, M.; Ye, J.; Huang, J.; Yang, X. Holey nitrogen-doped graphene aerogel for simultaneously electrochemical determination of ascorbic acid, dopamine and uric acid. *Talanta* **2021**, *224*, 121851. [CrossRef]
39. Fukuda, T.; Muguruma, H.; Iwasa, H.; Tanaka, T.; Hiratsuka, A.; Shimizu, T.; Tsuji, K.; Kishimoto, T. Electrochemical determination of uric acid in urine and serum with uricase/carbon nanotube/carboxymethylcellulose electrode. *Anal. Biochem.* **2020**, *590*, 113533. [CrossRef]
40. Thanh, T.S.; Qui, P.T.; Tu, N.T.T.; Toan, T.T.T.; Hoa, T.T.B.; Son, L.V.T.; Nguyen, D.M.; Tuyen, T.N.; Khieu, D.Q. Electrochemical determination of uric acid in urine by using zeolite imidazolate framework-11 modified electrode. *J. Nanomater.* **2021**, *2021*, e9914062. [CrossRef]
41. Tang, T.; Zhou, M.; Lv, J.; Cheng, H.; Wang, H.; Qin, D.; Hu, G.; Liu, X. Sensitive and selective electrochemical determination of uric acid in urine based on ultrasmall iron oxide nanoparticles decorated urchin-like nitrogen-doped carbon. *Colloids Surf. B* **2022**, *216*, 112538. [CrossRef] [PubMed]
42. Guo, H.; Liu, B.; Pan, Z.; Sun, L.; Peng, L.; Chen, Y.; Wu, N.; Wang, M.; Yang, W. electrochemical determination of dopamine and uric acid with covalent organic frameworks and Ox-MWCNT co-modified glassy carbon electrode. *Colloids Surf. A* **2022**, *648*, 129316. [CrossRef]
43. Stoikov, D.; Ivanov, A.; Shurpik, D.; Stoikov, I.; Evtugyn, G. Flow-through electrochemical biosensor with a replaceable enzyme reactor and screen-printed electrode for the determination of uric acid and tyrosine. *Anal. Lett.* **2022**, *55*, 1281–1295. [CrossRef]
44. Ivanov, A.; Stoikov, D.; Shafigullina, I.; Shurpik, D.; Stoikov, I.; Evtugyn, G. Flow-through acetylcholinesterase sensor with replaceable enzyme reactor. *Biosensors* **2022**, *12*, 676. [CrossRef]
45. Shamagsumova, R.V.; Kulikova, T.N.; Porfireva, A.V.; Shurpik, D.N.; Stoikov, I.I.; Rogov, A.M.; Stoikov, D.I.; Evtugyn, G.A. Electrochemistry and electrochemical assessment of host–guest complexation of substituted pillar[m]arene[n]quinones. *J. Electroanal. Chem.* **2023**, *938*, 117444. [CrossRef]
46. Smolko, V.A.; Shurpik, D.N.; Evtugyn, V.G.; Stoikov, I.I.; Evtugyn, G.A. Organic acid and DNA sensing with electrochemical sensor based on carbon black and pillar[5]arene. *Electroanalysis* **2016**, *28*, 1391–1400. [CrossRef]
47. Neghmouche, N.S.; Khelef, A.; Lanez, T. Electrochemistry characterization of ferrocene/ferricenium redox couple at glassy carbon electrode. *J. Fundam. Appl. Sci.* **2015**, *1*, 23–30. [CrossRef]
48. Zhang, Z.; Liang, H.; Li, M.; Shao, L.; Hua, B. Host–guest complexation of perethylated pillar[6]arene toward ferrocene derivatives both in solution and solid state: Different binding modes induced by minor structural changes of guests. *Org. Lett.* **2020**, *22*, 1552–1556. [CrossRef] [PubMed]
49. Liu, H.; Tian, Y.; Xia, P. Pyramidal, rodlike, spherical gold nanostructures for direct electron transfer of copper, zinc-superoxide dismutase: Application to superoxide anion biosensors. *Langmuir* **2008**, *24*, 6359–6366. [CrossRef] [PubMed]

50. Liu, J.; Yang, C.; Shang, Y.; Zhang, P.; Liu, J.; Zheng, J. Preparation of a nanocomposite material consisting of cuprous oxide, polyaniline and reduced graphene oxide, and its application to the electrochemical determination of hydrogen peroxide. *Microchim. Acta* **2018**, *185*, 172. [CrossRef]
51. Magro, M.; Baratella, D.; Pianca, N.; Toninello, A.; Grancara, S.; Zboril, R.; Vianello, F. Electrochemical determination of hydrogen peroxide production by isolated mitochondria: A novel nanocomposite carbon–maghemite nanoparticle electrode. *Sens. Actuators B* **2013**, *176*, 315–322. [CrossRef]
52. Lin, D.; Su, Z.; Wei, G. Three-dimensional porous reduced graphene oxide decorated with MoS_2 quantum dots for electrochemical determination of hydrogen peroxide. *Mat. Chem.* **2018**, *7*, 76–83. [CrossRef]
53. Pfrimer, P.; Moraes, L.M.P.; Galdino, A.S.; Salles, L.P.; Reis, V.C.B.; de Marco, J.L.; Prates, M.V.; Bloch, C.; Torres, F.A.G. Cloning, purification, and partial characterization of bacillus subtilis urate oxidase expressed in *Escherichia coli*. *J. Biomed. Biotechnol.* **2010**, *2010*, 674908. [CrossRef] [PubMed]